Journal of Thermal Engineering
Web page info: https://jten.yildiz.edu.tr
DOI: 10.18186/thermal.1278242

Research Article

Numerical investigation on the effect of slit thickness and outlet angle of the bladeless fan for flow optimization using CFD techniques

Dineshkumar RAVI[1], Thundil Karuppa RAJ RAJAGOPAL[1]*

[1]*School of Mechanical Engineering, Vellore Institute of Technology, Vellore, Tamil Nadu, 632014, India*

ARTICLE INFO

Article history
Received: 10 March 2022
Accepted: 24 July 2022

Keywords:
Air Multiplier; Coanda Effect; Computational Fluid Dynamics; Bladeless Fan; Aerofoil

ABSTRACT

The effect of outlet thickness and outlet angle of the bladeless fan have been an alysed numerically on the aerodynamic performance of the bladeless fan. Five different aerofoil profiles have been considered for the present work is Eppler 479, Eppler169, Eppler 473, S1046 and S1048. The bladeless fan arrangement has been achieved by converting the aerodynamic models listed above. The ANSYS ICEM CFD 16.0 have been used to discretize the enclosure and bladeless fan through finite volume approach. The mesh model is then imported into ANSYS CFX 16.0 pre-processor for applying the required boundary conditions. The governing equations namely continuity and momentum are used to solve the flow physics through and across the bladeless fan and SST k-? turbulence model has been used to predict the turbulence in the bladeless fan. The effect of outlet thicknesses and outlet angles have been varied for all the five aerofoil configurations mentioned and the volumetric flow at inlet have been adjusted from 5 LPS to 80 LPS. Outlet thickness is varied from 0.8, 1.0, 1.3, 1.5 and 2 mm and the slit angle is varied from 20 degrees to 80 degrees in step of 10 degrees. The results predicted that Eppler 473 aerofoil profile showed better performance when the thickness of slit and outlet angle has been fixed constant as 1 mm and 70 degree respectively. Also, the maximum discharge flow ratio is recorded for an inlet volumetric flow rate of 80 LPS and it is found to be 34.37. The present numerical study substantiated that outlet thickness plays a dominant role on the bladeless fan's aerodynamic performance compared to outlet angle and aerodynamic shape considered in this numerical analysis. The contours of velocity, streamline and pressure of the bladeless fan have been discussed.

Cite this article as: Ravi D, Raj Rajagopal T K. Numerical investigation on the effect of slit thickness and outlet angle of the bladeless fan for flow optimization using CFD technique. J Ther Eng 2023;9(2):279–296.

***Corresponding author.**
E-mail address: thundilr@gmail.com, rdinesh223@gmail.com

This paper was recommended for publication in revised form by Regional Editor Ahmet Selim Dalkilic

Published by Yıldız Technical University Press, İstanbul, Turkey
Copyright 2021, Yıldız Technical University. This is an open access article under the CC BY-NC license (http://creativecommons.org/licenses/by-nc/4.0/).

INTRODUCTION

The bladeless fan is completely different from that of conventional fans (i) no observable blades, (ii) working mechanism is entirely different, (iii) uniform distribution of airflow and (iv) noise generated by the bladeless fan is comparatively low. The bladeless fan or air multiplier is a device which consists of an aerodynamic ring, cylindrical tower, and centrifugal impeller. The concept of bladeless fan is new, and it is completely different from that of conventional fans. It does not have visible blades or impellers but whereas a small fan has been placed underneath the cylindrical base tower. In the year 2009, British company namely Dyson Limited, introduced the concept of an air-multiplier, commonly called as bladeless fan and which is currently manufactured for residential applications with hydraulic diameter not more than 300 mm [1]. Based on the flow direction, fans are often classified into two types are axial and radial fans. Axial fans have a fluid flow that is parallel to impeller's rotation axis. Axials fans are frequently utilized in domestic and low-pressure systems like cooling towers and wind tunnels. Axial fans have been shown to produce greater turbulence and noise, which is mostly caused by the space between housing and blade profile. The impellers were examined in various states: forward-skewed, backward-skewed and unskewed and based on their results they substantiated that forward skewed profile performed better than others and has a decreased noise, larger pressure coefficient and less turbulence. Generally, the radial fan fluid flow direction is perpendicular (90 degree) to the axis of rotation of blade profiles. Radials fans are most widely used in high pressure conditions and hence, it is most commonly used in applications like HVAC systems. The vortex formation and obstruction in the blade channel, causes an unstable flow pattern and noise generation, were the key factors affecting the aerodynamic and aeroacoutics performance of a radial impeller. It was found that when the blade wrap angle was optimized, vortices' size decreases with decreased sound pressure level, where the rest of the design parameters are constant [3]. They reported that adding extended surfaces to the radial impeller's trailing edge can improve a radial fan's performance. The results exhibited that a radial fan with extended surface on blade impeller performed better in terms of volumetric flow rate, pressure, power available in the shaft, and noise level increases while the efficiency of radial fan decreases. When the conventional blade profiles were replaced with the aforementioned, the maximum sound pressure values spiked from 88.5 dB to 92.5 dB, respectively. A decrement of 27% of volute was obtained when extended surfaces are used which causes noise level to rise initially. Further the volumetric flow rate increases, while the impeller's noise level decreases noticeably [4]. Moosania et al., (2021) have carried out a numerical investigation on the effect of flow field in an unshrouded, partially, and fully shrouded fan to understand the effects of radial inlet flow on the main flow and the flow in the tip region. A partial shrouded fan is a type of axial fan that has a partial shroud or cover around the rotor, which can affect the flow of air and the fan's performance. They revealed that fully shrouded fan provided a better performance than partially shrouded and unshrouded fan. They also reported that in low pressure rise conditions, the axial inlet flow with partially shrouded fan have the same scale as that of the radial fans. In partially shrouded fan, blockage and reverse flow can be reduced by changing the magnitude of tip leakage vortex leaving the fan, trajectory and location of the fluid flow and also, the tip leakage vortex loss is the main loss mechanism which involved in the partially shrouded fan whereas in the fully shrouded fan, the hub also plays a key role apart from the tip leakage vortex loss. They concluded that though the partially shrouded fan provided a lower performance than fully shrouded, it is most widely used in air conditioning system due to its larger inlet area which allows the installation of bigger upstream heat exchanger [5]. Compared to air multipliers, conventional fans have visual external blades that pose a risk to pets and children. The conventional fans generate air due to cutting action and which generates more noise and unpleasant feeling to the user and also the maintenance and cleaning of blades are difficult. In comparison to a traditional fan, a bladeless fan requires a much smaller fan to provide the same output. A tiny centrifugal fan has been placed near the bottom surface of cylindrical tower that pulls air from the surrounding area of bladeless fan and forced to flow it into the bladeless fan slit, and then comes out with high velocity. The air that emerges through the bladeless fan's slit has a greater tendency to adhere to curved surfaces and develops a pressure drop between the bladeless fan system and surroundings of a bladeless fan and this phenomenon of staying adhere to the curvature is called as Coanda effect [6]. Guoqi Li et al. [7] have conducted a two-dimensional numerical investigation and they have discussed the effect of the bladeless fan's aerodynamic shape. They have modified the bottom curvature of the selected aerofoil have been analysed for five different configurations. They have developed an experimental prototype of the same and has compared with one of curvature blade profiles for validating the numerical code. They have reported that increasing the curvature of bottom surface increases the velocity gradient, flow and maximum average velocity near the coanda region. Multiple low-pressure regions have emerged as the bladeless fan curvature outgrows a critical limit, eventually joins together to form a large low-pressure region. This low-pressure zone in the core region induces increased air flow from the bladeless fan surroundings to flow with the direction parallel to the air flow. Hence, they reported that the bladeless fan performance and flow behaviour are greatly influenced by the aerofoil's curvature [6]. In the current numerical investigation, large curvature profiles of S1046, S1048, Eppler169, Eppler479 and Eppler473 are selected

and the same have been modified into a complete bladeless fan arrangement with varying configurations. Jafari and group [8] have carried out numerical investigation on the effect of various design parameters on the performance of an Eppler473 aerodynamic profile. They have selected various design parameters namely, slit width, aspect ratio, outlet angle, and hydraulic diameter. They revealed that outlet thickness is the key parameter compared to other design parameters considered for their study. They substantiated that the volumetric air at outlet increases by roughly 12.5 to 25 times more than that at the inlet when the thickness of the slit is reduced from 3 to 1 mm. The same research group in the year 2017 [9] had numerically analysed the impact of aeroacoustic and aerodynamic performance on the scaled up model of a bladeless fan for domestic and industrial applications. They have carried out aerodynamic and aeroacoutics validation by developing an experimented prototype of a bladeless fan where the hydraulic diameter is maintained as 600 mm and they have compared the experimented results with numerically predicted values of volumetric flow rate and sound pressure level respectively. The experimental and numerical results provided a close agreement between the two. They reported that increasing the hydraulic diameter of a bladeless fan provides a great control in adjusting the volumetric flow rate and this make it suitable for domestic and industrial use. Hong et al. [10] have performed numerical investigation on the effect of flow-field of a bladeless fan. They have varied the Reynolds number between 28200 and 40100 based on turbulent jet theory. By changing the inlet Reynolds number, they plotted the turbulent intensity and time averaged velocity in both the vertical (z/d) and horizontal (y/d) flow directions at various axial points (x/d). They reported that increasing inlet Reynolds number has increased these parameter effectively. They reported that when the axial distance reaches 1.5 times the diameter of bladeless fan, flow field starts to converge. This clearly indicates that lower fluid flow lines converge to move up and mixing of these two happens at a distance of 1.5d. As the axial distance from leading edge of a bladeless fan has increased up to $3D_h$ (hydraulic diameter), the mixing of lower part terminated and forms a classical single jet and it was observed that velocity peak values started decaying. Beyond the axial site of 3.5 times of its hydraulic diameter of a bladeless fan, a field of axisymmetric flow with time-averaged velocity and intense turbulent flow was observed.

Jafari et al. [11] had carried out a numerical analysis on the aeroacoustic and aerodynamic performance of a bladeless fan. The Eppler473 aerofoil was chosen as a cross-section for the bladeless fan aerodynamic profile, which has a chord length of 100 mm, a hydraulic diameter of 30 cm, and an outlet thickness of 1.3 mm. They reported that continuity and momentum equations are used to capture the fluid flow variations and the Shear Stress Transport (k-?) turbulence model in order to capture the turbulence effects. The Broadband Noise Source (BNS) is mainly applied for steady state approach and the Ffowcs Williams and Hawkings model for time dependent transient conditions, in order to predict the aeroacoustic characteristics numerically. The BNS model is used to identify the noise source and FW-H model is used to predict the noise level generated for different inlet volumetric flow rates and they also found that linear agreement was found between the inlet and outlet volumetric flow rates. The maximum discharge flow ratio was found to be as high as 21. They found that the outlet slit is the main source of noise, and that the sound pressure level rises from 40 dB to 80 dB when the input flow rate rises from 10 LPS to 80 LPS. Chou et al., [12] performed a numerical investigation on the effect of turbulence flow past a bladeless fan. The cross-section for the bladeless fan was chosen from two different aerofoils. They have selected E473 aerofoil cross section as top section and NACA 4412 as the bottom section. They have reported that increasing the inlet Reynolds number and diameter of bladeless fan have increased the discharge flow ratio significantly. They found that the bladeless fan's inlet flow rate and hydraulic diameter have a significant impact on its performance, whilst the remaining parameters have very little effect on outlet volumetric flow rate. Mehmood et al [13] performed a three dimensional numerical analysis on bladeless fan as an effective replacement to domestic ceiling fan. It is observed that peak velocity in the core region has increased upto 33% when hydraulic diameter of a bladeless fan has increased from 30 cm to 50 cm. A numerical investigation on a new suction-hood model which enables the total disposal of gases created while cooking was conducted by Carlini et al. [14]. They have proposed two innovation air capture systems namely airflow amplifier and bladeless fan systems as new suction hood model. They have created a parametric sweep function in order to identify the system behaviour on various input conditions. The velocity, extension of ejector and flow rate have been recorded and analysed. They demonstrated the viability of the new suction systems, which consumed energy less than other ventilation systems of today. Aslam et al [15] have carried out a two-dimensional numerical analysis on the performance of a aerofoil-based bladeless ceiling fan. They have selected E473 aerodynamic profile as the cross section and they also considered various geometrical parameters namely, fan's hydraulic diameter, nozzle diameter and height from the ceiling on volumetric flow rates. They have revealed that volumetric flow rate of the bladeless fan has increased till 300 mm away from the ceiling and it tends to decrease beyond 300 mm. They have also reported that discharge coefficient increases with increase of fan diameter. From the literature, it is observed that very few researches have been done that involves both numerical and experimental work on the geometrical characteristics of a single aero foil "NACA 4 digit" and "Eppler 473"series in the area of the bladeless fan. The selection of aerodynamic profile for the bladeless fan is not same for

each Reynolds number with respect to the lift to drag ratio. To address the research gap optimization of aerofoil selection is based on Reynolds number ranging between 2 X 10^5 and 5 X 10^5. The research work has also been extended to optimize the various design parameters like outlet thickness and outlet angle (also called as slit angle) of the aerodynamic profiles.

The bladeless fan's performance is the subject of a three-dimensional numerical investigation in this study. The cross section of the aerofoil has been selected based on the lift to drag ratio for different Reynolds number and good coanda surface. Aerodynamics profiles namely, Eppler169, Eppler473, Eppler479, S1046, and S1048 are the five aerofoils that were taken into consideration for the present numerical study. The influence of geometrical parameters like outlet thickness and outlet angles for all the above mentioned aerofoil profiles are numerically investigated. The outlet thicknesses have been adjusted from 0.8 mm, 1 mm, 1.3 mm, 1.5 mm and 2 mm and the outlet angles have been adjusted from 20 degree to 80 degree with intervals of 10 degree for all the above mentioned aerofoils. The chord length, hydraulic diameter and aspect ratio have been maintained as 100 mm, 300 mm and 1 respectively for all the numerical cases considered

Table 1. Comparison of similar research work carried out by various authors

S.No	Proposed study	Parameters	Inference	References
1	Numerical investigation of geometric parameter effects on the aerodynamic performance of a Bladeless fan	Profile Considered: Eppler473 1. Thickness of the slit 2. Hydraulic diameter 3. Outlet angle 4. Aspect ratio	Reducing the thickness of the slit provided a significant improvement in the discharge flow ratio and performance of a bladeless fan. Similarly, reducing the outlet angle provided an improvement in the discharge flow ratio The discharge flow ratio increases with increase of hydraulic diameter (D_h) of the bladeless fan The optimal aspect ratio is found to be 1. Increasing it further decreases the performance.	[7, 16]
2	Experimental and numerical investigation of a 60cm diameter bladeless fan	Profile Considered: Eppler473 Hydraulic Diameter = 60 cm	The discharge flow ratio increases with increase of hydraulic diameter (D_h). Increasing the inlet volumetric flow has increased noise generated by bladeless fan system	[8]
3	Experimental investigation on the outlet flow field structure and the influence of Reynolds number on the outlet flow field for a bladeless fan	Five Reynolds numbers considered in the present study are 28200, 30900, 34000, 37000 and 40100	Increasing the Reynolds number from 28200 to 40100 increases the time-averaged velocity in axial and radial direction. The flow-field tends to converge at axial distance of 1.5 times of its hydraulic diameter of the bladeless fan for all the Reynolds number. The flow field saturates when the axial distance from the bladeless fan reaches 3d.	[8]
4	Numerical Aerodynamic Evaluation and Noise Investigation of a Bladeless Fan	Profile Considered: Eppler473 Hydraulic Diameter = 30 cm	For domestic use, hydraulic diameter (D_h) has been maintained as 30 cm for the bladeless fan The maximum discharge flow ratio was recorded as 21 for E473 at 80 Lps The noise investigation results predicted that increasing inlet volumetric flow rate has increased the noise level by the bladeless fan.	[10]
5	Numerical analysis of bladeless ceiling fan: An effective alternative to conventional ceiling fan	Profile Considered: Eppler473 Hydraulic Diameter = 30 cm	It is observed that peak velocity in the core region has increased upto 33% . When the hydraulic diameter (D_h) of a bladeless fan has increased from 30 cm to 50 cm.	[12]

in this study. The volumetric flow rate at inlet has been adjusted from 5 LPS to 80 LPS for all configurations mentioned above and the numerically predicted results have been discussed and presented. The variation of discharge flow ratio with respect to outlet thickness and outlet angles have been provided for various volumetric flow rates at inlet. The streamlines, velocity vector, velocity and pressure plot have been provided and discussed for better understanding of the fluid flow physics through and across the bladeless fan

MECHANISM OF A BLADELESS FAN

The complex flow physics through the three dimensional bladeless fan involves five different steps starting from inlet to exit as shown in Figure 1. It has been suggested by Nicholas et al. [1] that the volumetric flow rate at the exit should be measured from the leading edge of the bladeless fan to an axial-distance of 3 times of the bladeless fan diameter. Hong et al. [10] also numerically investigated and predicted that when the distance between the leading edge of the bladeless and 3Dh of its diameter, flow field starts to converge and when the distance between the two exceeds 3d, the flow field saturates and the peak velocity in the core region tends to decrease and it reaches a similarity state thereafter. Hence, it has been found from the literature that the volumetric flow rate of a bladeless fan should be measured from a distance of 3 times of its diameter from leading edge.

The working principle of a bladeless fan involves four different steps. The first step involves the collection of inlet air from the atmosphere and which is then allowed to pass through a cylindrical tower using a centrifugal fan of smaller capacity as shown in Figure 1. The inlet volumetric flow rate has been calculated numerically just above this small centrifugal fan. The second stage involves the distribution of collected inlet air through an aerodynamic structure. The aerodynamic structure consists of a throat region, divergent region at the trailing edge and a small slit. Generally, the outlet thickness has been maintained between 1 mm and 2 mm. Since, outlet thickness is very small, the collected inlet air comes out from the slit with a high velocity. The third stage involves the suction air, the high jet velocity from the slit develops a low pressure region inside the aerodynamic ring, the pressure drop between the atmosphere and aerodynamics ring forces air from the atmosphere and forced to flow in the direction of airflow. This type of air inducement is called the suction air; the air multiplied through suction mechanism is nearly 15 to 20 times of the inlet air. The fourth stage involves the entrainment air, Due to viscous shearing; the surrounding air that flows past the aerodynamic ring also starts to flow in the direction of air flow. This sort of air multiplication results in entrainment air, as seen in Figure 1. The step 5 indicates the overall working mechanism of the bladeless fan involving inlet air, suction air and entrainment air.

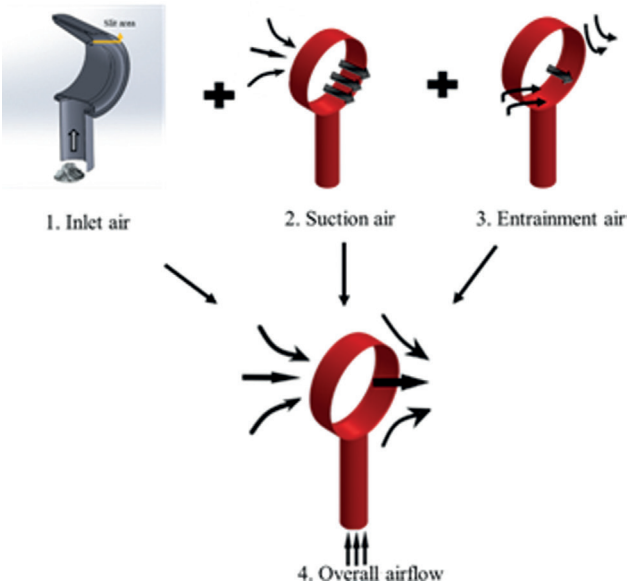

Figure 1. Working mechanism of a bladeless fan setup.

NUMERICAL METHODOLOGY

The present study investigates the effect of outlet thickness and outlet angle of a bladeless fan. The numerical analysis of a bladeless fan involves three different stages, pre-processing, solving and post-processing. The pre-processing stage involves, modelling, discretizing and setting up proper boundary conditions. Five different aerodynamic profiles have been considered as the bladeless fan cross-section namely, S1046, S1048, E169, E479 and E473. The selected aerodynamic profiles along with enclosure have been modeled using solid works 14.0 design modeler. The thickness of the slit has varied between 0.8 mm, 1 mm, 1.3 mm, 1.5 mm and 2 mm. The bladeless fan's outlet angle has varied from 20 degrees to 80 degrees. The bladeless fan and also the enclosure have been tetrahedrally discretized with finite volume method. Ansys CFX 16.0 is used to apply the required boundary values for the mesh model. The second phase in this numerical analysis involves solving the required governing equations of continuity and momentum for predicting the behaviour of fluid flow. The turbulence induced by the air multiplier and enclosure have been captured using SST k-? model. The residuals of mass, momentum and turbulence are fixed at 10^{-6}. At the outlet plane, a volumetric flow rate monitoring point has been created and monitored for every iteration till it reaches a similarity state. A total number of 500 iterations has been chosen for this numerical study, and

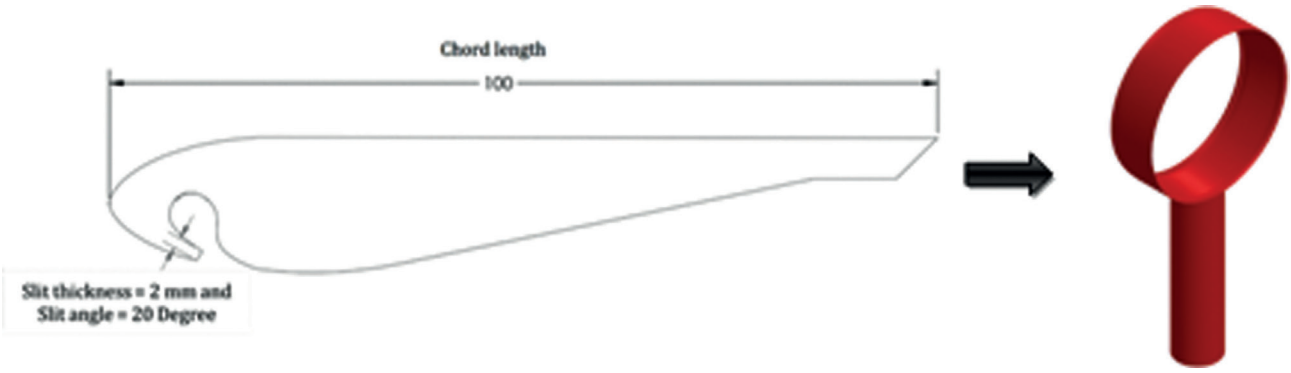

Figure 2. a) Aerofoil Eppler 473 cross section model, b) Three dimensional bladeless fan model.

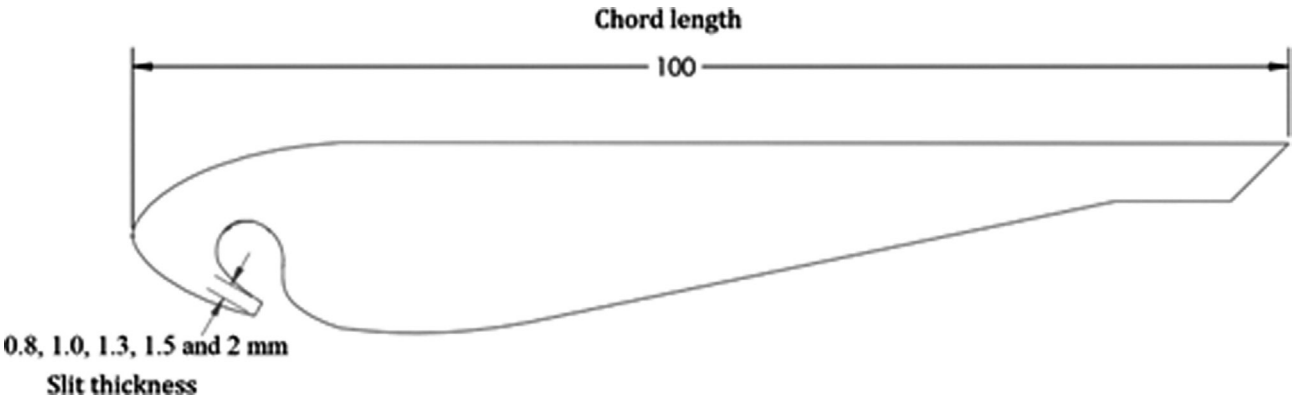

Figure 3. Aerofoil cross-section model for E473 with outlet thicknesses (0.8 mm, 1 mm, 1.3 mm, 1.5 mm, and 2 mm).

the convergence was achieved between 250 and 300 iterations for various design models and boundary conditions. The final stage of the study involved plotting the velocity, streamline and pressure contours for various aerodynamic profiles, outlet thicknesses and outlet angles for the bladeless fan and to identify the best suitable configuration for domestic use.

Numerical modelling

The present study, aerofoils have been selected based on its thickness and high lift to drag ratio for various Reynolds numbers ranging from 2 x 10^5 to 5 x 10^5. A total number of 5 different aero-foils have been considered for the present numerical study namely, Eppler169, Eppler473, Eppler479, S1046 and S1048. The Eppler 473 aerodynamic cross section as shown in Figure 2a has been transformed into a complete numerical model of bladeless fan using Solid works 14.0 modeller as given in Figure 2b. The geometrical parameters of the bladeless fan considered for the numerical work are outlet thickness and slit angle. The outlet thickness is varied between 0.8, 1.0, 1.3, 1.5 and 2.0 mm as shown in Figure 3 corresponding to five different configurations for a single aerofoil. The slit angle has also been varied between 20°, 30°, 40°, 50°, 60°, 70°, and 80° as shown in Figure 4 for all the above five outlet thickness configurations. Hence the total number of numerical simulations for a single aero foil leads to 35 different numerical investigations for a particular value of Reynolds number. In this numerical study, overall five different aerofoils have been considered which leads to 175 numbers of various numerical simulations for the given Reynolds number as given in Table 2. In the present work, the volumetric flow rate at inlet has been varied from 5 LPS and 80 LPS which corresponds to a total 1400 numerical simulations. The aspect ratio, hydraulic diameter and chord length has been maintained as 1, 30 cm, and 10 cm respectively for all the 1400 numerical simulations.

Using Solid Works 16.0 assembly, the bladeless fan's three-dimensional numerical model and the enclosure have been added into a single assembly file, as shown in Figure 5. For the purpose of this investigation, an enclosure with dimensions of 8000 mm x 4000 mm x 4000 mm. The height and diameter of the cylinder has been maintained as 9 cm and 50 cm respectively.

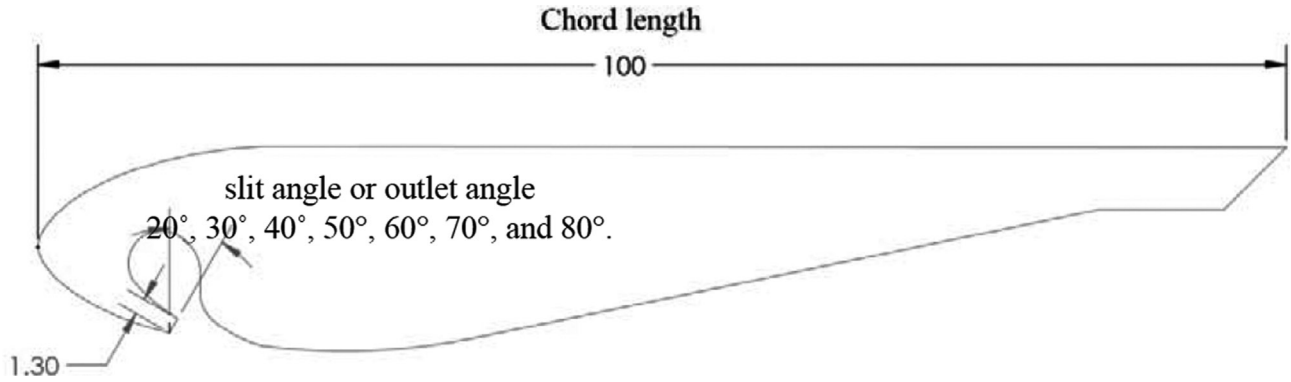

Figure 4. Aerofoil cross-section model for E473 with slit-angles (20°, 30°, 40 ° 50°, 60°, 70°, and 80°).

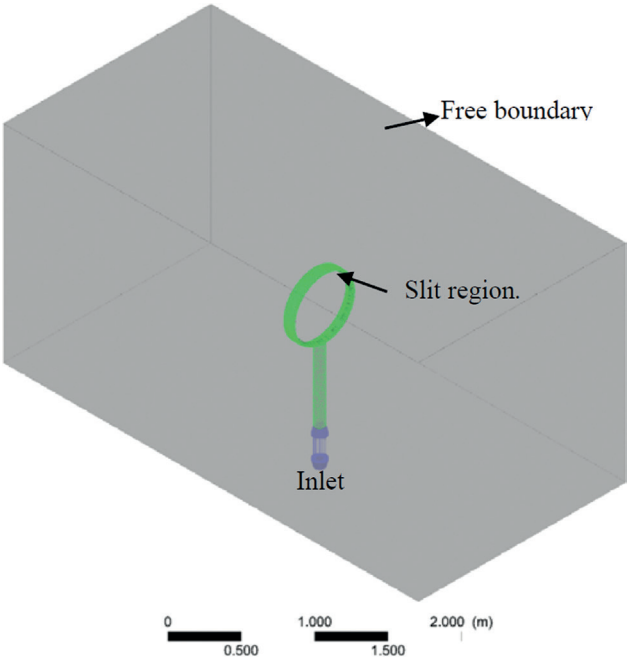

Figure 5. 3D – simple representation of enclosure and bladeless fan numerical model.

Discretization

Using a finite volume approach, the enclosure and bladeless fan have been tetrahedrally discretized into nearly 712,235 elements. A face sizing technique has been opted to discretize the enclosure and bladeless fan domain. The sizing of inlet, outer surface of aerodynamic ring, outer surface of base tower, opening surface and slit area have been selected as 10 mm, 3 mm, 5 mm, 50 mm and 0.18 mm respectively as shown in Figure 6. The bladeless fan mesh model is shown in Figure 7 and the half-sectional view of fan slit region is shown in Figure 8. The discretized model of enclosure and bladeless fan is combined into a single mesh file using ANSYS ICEM CFD 16.0 and the same has been converted into unstructured grid format for ANSYSCFX 16.0 for setting up the boundary values as shown in Table 3.

Mesh Sensitivity test

The grid independence study also called mesh sensitivity test are used to make sure that the expected numerical values are unaffected by the number of elements. The volumetric flow rate at the enclosure outlet for an Eppler473 aerofoil with a 1mm outlet thickness and a 70° outlet angle have been compared and presented in the present work for various number of elements ranging from 2.75 million to nearly 10 million tetrahedral elements. For the purposes of this validation study, the inlet volumetric flow rate has been fixed as 5 LPS. It has been noted that the volumetric flow rate at the meridian plane increases from 102 LPS to 112 LPS, which yields to a maximum deviation of about 10%, when the grid size is increased from 2.75 million to 7.2 million. The volumetric flow rate at meridian plane did not significantly change when the number of elements was extended beyond 7.2 million elements, to 8.49 million and nearly 10 million, as shown in Figure 10. When the number of elements is extended above 7.2 million tetrahedral elements, there is a smaller than 0.08% difference in the volumetric flow rate at the meridian plane. In order to improve accuracy and decrease computation time for the work, the grid size has been optimised to roughly 7.2 million for all the 1400 numerical simulations.

Mathematical modelling and solution technique

The mathematical modelling and solution technique involves in solving the governing equations to numerically predict the flow variables. For the present numerical work various design parameters have been considered namely, aerodynamic profile, outlet thickness and outlet angle have been solved using ANSYS-CFX 18.0 Software. The governing equations namely, continuity and momentum have been

Table 2. Geometrical parameters taken into consideration for this investigation

No. of Cases	Aerofoil shape	Outlet thickness	Slit angle
1-7	Eppler 169	0.8 mm	20˚, 30˚, 40˚, 50˚, 60˚, 70˚, 80˚
8-14	Eppler 169	1.0 mm	20˚, 30˚, 40˚, 50˚, 60˚, 70˚, 80˚
15-21	Eppler 169	1.3 mm	20˚, 30˚, 40˚, 50˚, 60˚, 70˚, 80˚
22-28	Eppler 169	1.5 mm	20˚, 30˚, 40˚, 50˚, 60˚, 70˚, 80˚
29-35	Eppler 169	2.0 mm	20˚, 30˚, 40˚, 50˚, 60˚, 70˚, 80˚
36-42	Eppler 473	0.8 mm	20˚, 30˚, 40˚, 50˚, 60˚, 70˚, 80˚
43-49	Eppler 473	1.0 mm	20˚, 30˚, 40˚, 50˚, 60˚, 70˚, 80˚
50-56	Eppler 473	1.3 mm	20˚, 30˚, 40˚, 50˚, 60˚, 70˚, 80˚
57-63	Eppler 473	1.5 mm	20˚, 30˚, 40˚, 50˚, 60˚, 70˚, 80˚
64-70	Eppler 473	2.0 mm	20˚, 30˚, 40˚, 50˚, 60˚, 70˚, 80˚
71-77	Eppler 479	0.8 mm	20˚, 30˚, 40˚, 50˚, 60˚, 70˚, 80˚
78-84	Eppler 479	1.0 mm	20˚, 30˚, 40˚, 50˚, 60˚, 70˚, 80˚
85-91	Eppler 479	1.3 mm	20˚, 30˚, 40˚, 50˚, 60˚, 70˚, 80˚
92-98	Eppler 479	1.5 mm	20˚, 30˚, 40˚, 50˚, 60˚, 70˚, 80˚
99-105	Eppler 479	2.0 mm	20˚, 30˚, 40˚, 50˚, 60˚, 70˚, 80˚
106-112	S1046	0.8 mm	20˚, 30˚, 40˚, 50˚, 60˚, 70˚, 80˚
113-119	S1046	1.0 mm	20˚, 30˚, 40˚, 50˚, 60˚, 70˚, 80˚
120-126	S1046	1.3 mm	20˚, 30˚, 40˚, 50˚, 60˚, 70˚, 80˚
127-133	S1046	1.5 mm	20˚, 30˚, 40˚, 50˚, 60˚, 70˚, 80˚
134-140	S1046	2.0 mm	20˚, 30˚, 40˚, 50˚, 60˚, 70˚, 80˚
141-147	S1048	0.8 mm	20˚, 30˚, 40˚, 50˚, 60˚, 70˚, 80˚
148-154	S1048	1.0 mm	20˚, 30˚, 40˚, 50˚, 60˚, 70˚, 80˚
155-161	S1048	1.3 mm	20˚, 30˚, 40˚, 50˚, 60˚, 70˚, 80˚
162-168	S1048	1.5 mm	20˚, 30˚, 40˚, 50˚, 60˚, 70˚, 80˚
169-175	S1048	2.0 mm	20˚, 30˚, 40˚, 50˚, 60˚, 70˚, 80˚

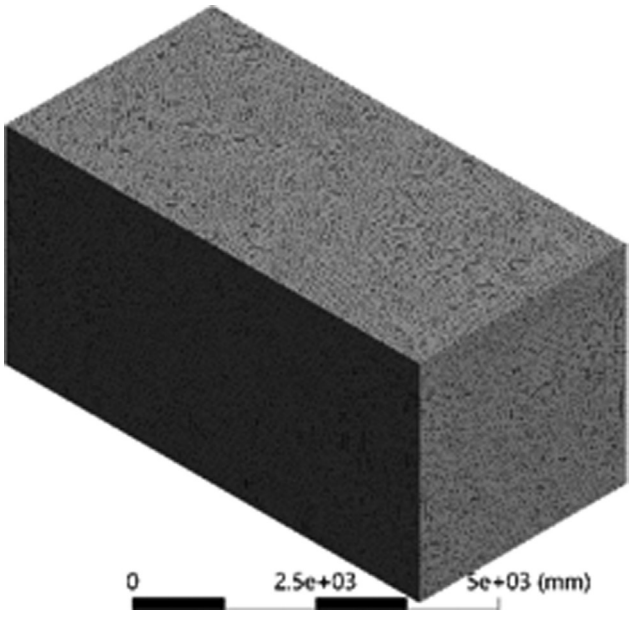

Figure 6. Discretization model of enclosure.

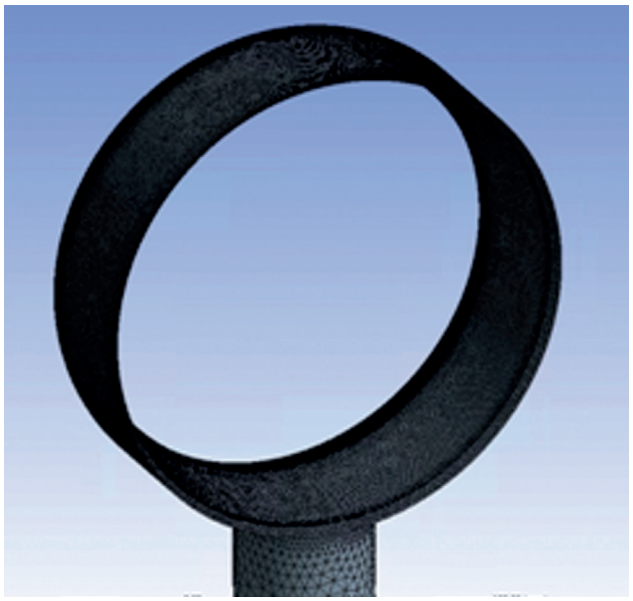

Figure 7. Enlarged view of discretized model of bladeless fan.

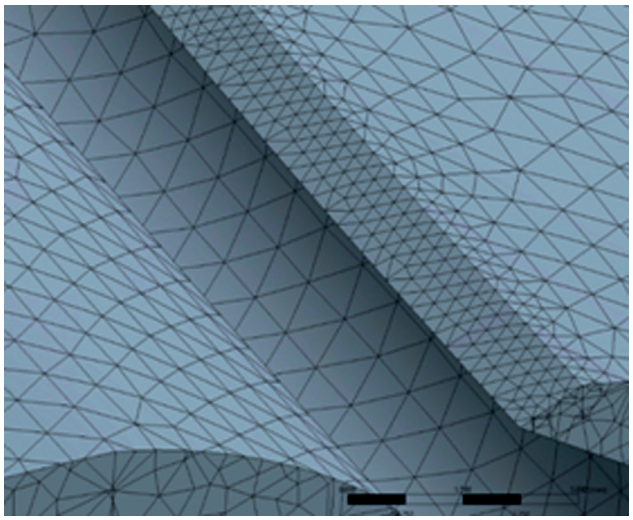

Figure 8. Sectional discretized model of a bladeless fan.

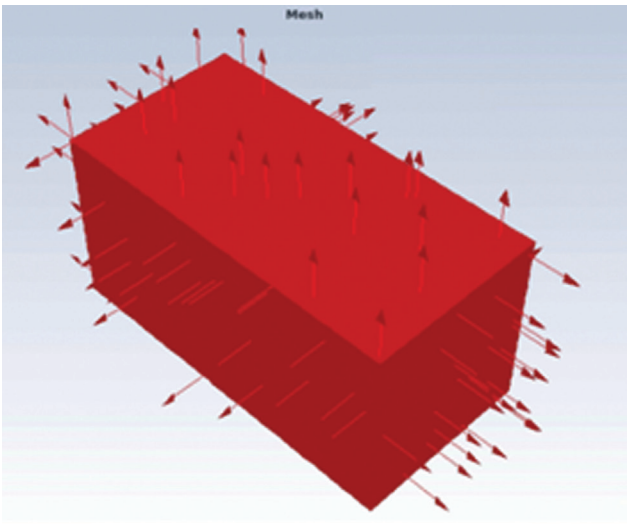

Figure 9. Discretized model of enclosure and bladeless fan.

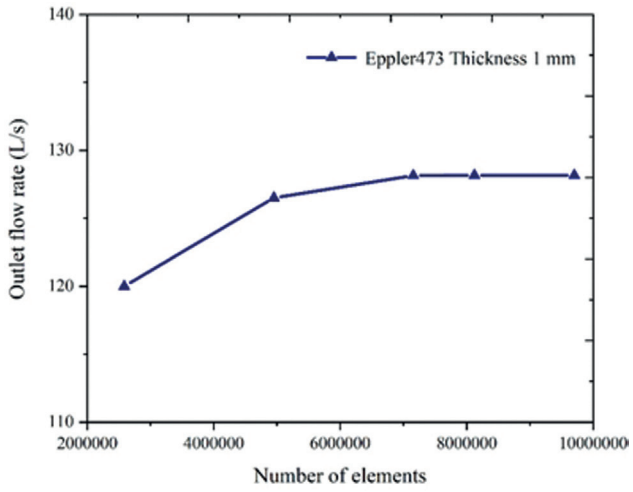

Figure 10. The effect of grid size on the outlet flow rate for a volumetric flow rate of 5 LPS.

solved to capture the fluid flow variations three dimensionally. By resolving the Shear Stress Transport (SST) k-mode of closure, the flow turbulence that was created has been captured. The enclosure and bladeless fan for all the configurations have been solved by using the governing equations listed below for the mentioned boundary values as shown in Table 3.

Continuity Equation:

$$\frac{\partial u}{\partial x}+\frac{\partial v}{\partial y}+\frac{\partial w}{\partial z}=0 \tag{1}$$

Momentum Equation:

The velocity component's scalar momentum equation in the x direction is provided by

$$\rho\left(u\frac{\partial u}{\partial x}+v\frac{\partial u}{\partial y}+w\frac{\partial u}{\partial z}\right)=-\frac{\partial P}{\partial x}+\frac{\partial}{\partial x_j}\left[(\mu+\mu_T)\left(\frac{\partial u}{\partial x_j}+\frac{\partial u_j}{\partial x}\right)\right], \tag{2}$$

The velocity component's scalar momentum equation in the y direction is provided by

$$\rho\left(u\frac{\partial v}{\partial x}+v\frac{\partial v}{\partial y}+w\frac{\partial v}{\partial z}\right)=-\frac{\partial P}{\partial y}+\frac{\partial}{\partial x_j}\left[(\mu+\mu_T)\left(\frac{\partial v}{\partial x_j}+\frac{\partial u_j}{\partial y}\right)\right], \tag{3}$$

The velocity component's scalar momentum equation in the y direction is provided by

$$\rho\left(u\frac{\partial w}{\partial x}+v\frac{\partial w}{\partial y}+w\frac{\partial w}{\partial z}\right)=-\frac{\partial P}{\partial z}+\frac{\partial}{\partial x_j}\left[(\mu+\mu_T)\left(\frac{\partial w}{\partial x_j}+\frac{\partial u_j}{\partial z}\right)\right], \tag{4}$$

Model of turbulence with k and omega transport equation:

The typical k-ω equation model's turbulent kinetic energy "k" is provided by

$$\rho\left(u\frac{\partial k}{\partial x}+v\frac{\partial k}{\partial y}+w\frac{\partial k}{\partial z}\right)=\frac{\partial}{\partial x_j}\left[\left(\mu+\frac{\mu_T}{\sigma_{k3}}\right)\frac{\partial k}{\partial x_j}\right] + P_k-\beta\rho k\omega, \quad (5)$$

The typical k-ω equation model's turbulent dissipation rate "ω" is provided by

$$\rho\left(u\frac{\partial w}{\partial x}+v\frac{\partial w}{\partial y}+w\frac{\partial w}{\partial z}\right)=\frac{\partial}{\partial x_j}\left[\left(\mu+\frac{\mu_T}{\sigma_{k3}}\right)\frac{\partial k}{\partial x_j}\right] + 2(1-F_1)\rho\frac{1}{\sigma_{w2}\omega}\frac{\partial k}{\partial x_j}\frac{\partial \omega}{\partial x_j}+\alpha_3*\frac{\omega}{k}P_k-\beta\rho\omega^2 \quad (6)$$

The expression for the turbulent viscosity (μ_T) is expressed as:

$$\mu_T=\rho\frac{k}{\omega} \quad (7)$$

Where u, v and w represents the x-component, y-component and z-component velocity, ρ represents the air density, F represents the blending function.

Boundary conditions required for Bladeless fan

The boundary values required for the present numerical work have been presented in Table 3. The volumetric flow rate at inlet has been varied from 5 LPS to 80 LPS (5, 20, 30, 40, 50, 60, 70, and 80 LPS). A tiny centrifugal fan with a capacity of 10 times smaller in size of conventional fan has been used to provide the inlet air at the cylinder base. All the outer surfaces except the bottom surface of the enclosure have been maintained as free boundary (atmospheric pressure) whereas the bottom surface of the enclosure have been maintained as wall. Similarly, the bladeless fan outer surface and cylinder outer surface have been maintained as wall with no slip assumption. The enclosure and bladeless fan has been divided into two different domains to have a better control on optimizing the grid sizes. In order to have continuity between the two domains, an interface boundary has been created between the enclosure slit surface and bladeless fan slit surface to establish the continuity between them. For the present numerical simulations following assumptions are made without sacrificing the accuracy of the predicted numerical results. The assumptions are fluid is steady and incompressible, the fluid is viscous and turbulent, gravity effect is neglected and the hydraulic diameter has been maintained as 300 mm.

Table 3. Appropriate boundary values for a bladeless fan

Name	Condition
Inlet	Volumetric flow Inlet – 5–80 LPS
Left, Right, Top, Front & Back	Opening – Atmospheric
Bottom & Outer wall	Smooth wall
Slit (Inner and Outer Domain)	Interface (Inner to outer domain)

NUMERICAL VALIDATION

The validation of numerical code in the present work has been done in two stages. In the first step, aerodynamic validation has been carried out with reference to Jafari et al., [10]. The C_L and C_D have been compared and presented against various angle of attack values ranging between -14.5 degree to 14.5 degree for a NACA 0012 aerofoil profile using ANSYS Fluent 18.0 and the numerically predicted values of lift and drag has been compared with the literature [10]. In the second step, fluid flow has been validated using velocity decay along streamwise direction and compared the same with the available literature [11].

The present numerically simulated results of fluid flow characteristics and aerodynamic charactersitics are matching closely with the literature. Jafari et al. [10] used a similar validation strategy, and the same strategy was used to validate the numerical code in their study and hence, the same approach has been used to validate the numerical code for the present work.

Aerodynamic Validation

The lift coeffcient (C_L) and drag coefficient (C_D) values of NACA 0012, which were predicted numerically, have been presented with reference to Jafari et al [10]. The boundary values used in this numerical simulation are identical to those used in the literature. [10]. The enclosure with dimensions of 3000 mm x 3000 mm and an aerofoil chord-length of 100 mm have been used in the numerical simulation to validate the aerodynamic characteristics. The Reynolds number at inlet has been maintained as $3e^6$. The numerical model of aerofoil profile along with enclosure is hexahedrally discretized through finite volume approach. The C_L and C_D has been compared and presented against the angle of attack as shown in Figure 11 and Figure 3 and the same has been compared with the literature [10]. The NACA 0012 aerofoil's C_L variation against the angle of attack is shown in Figure 11. The predicted values closely matched those of the literature, with the highest variance being less than 1.53% for an angle of attack of 14.5°. However, as depicted in Figure12, the numerically simulated coefficient of drag of this simulation slightly deviate from those of the literature but well within acceptable limits. A similar trend in coefficient of drag has been noted from the literature as well.

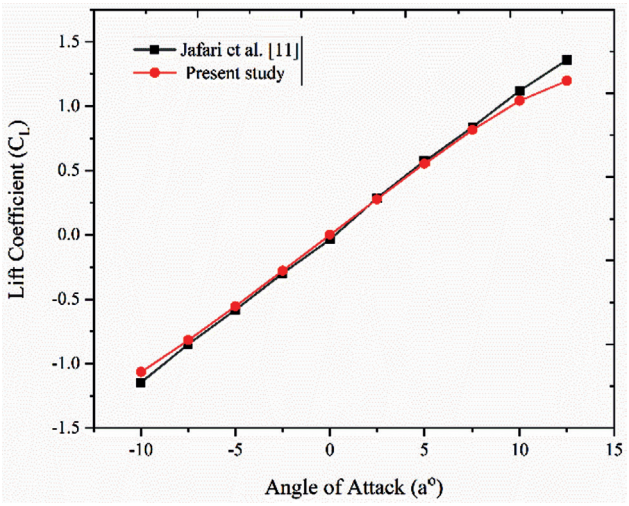

Figure 11. Coefficient of lift (C_l) and angle of attack comparison of NACA 0012.

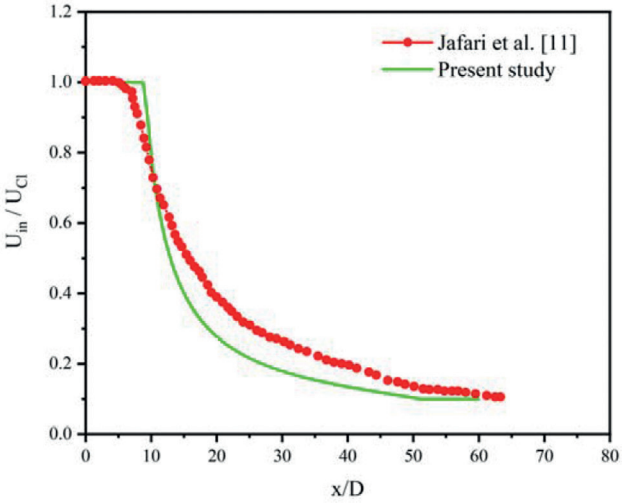

Figure 13. Velocity decay plot in the streamwise direction.

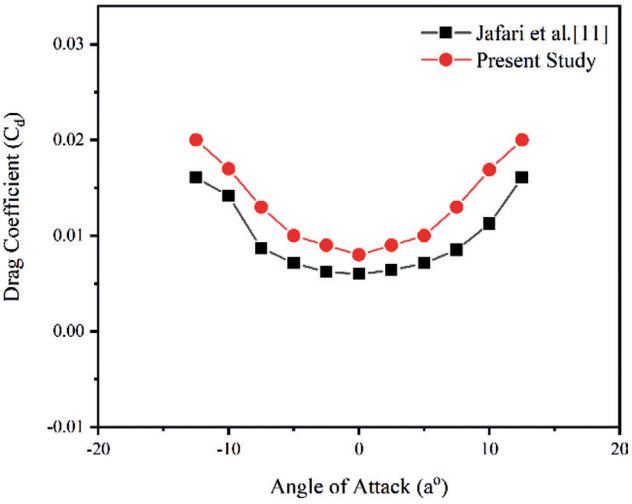

Figure 12. Coefficient of drag (C_d) and angle of attack comparison of NACA 0012.

Flow Validation

The fluid that emerges from the bladeless fan's small opening behaves like a jet flow. And hence, the circular jet-flow along the cylinder presented in the literature [10] is the focus of the second validation stage. The diameter of jet surface has been maintained as 1 cm, length and outer diameter of the cylinder has been maintained as 10 cm and 2 cm respectively. as given in the literature. The numerical analysis has been assumed to be axisymmetric as described in the literature [10] in order to cut down on computational time. A velocity boundary condition of nearly 60 m/s exists at the inlet and pressure outlet boundary condition with 1 atmospheric pressure has been assigned to the exit. It has been assumed that the cylindrical tube's outer surface is symmetric. The numerically projected streamwise velocity-decay values through the jet-centerline has been presented and compared to the data reported in the literature [10] as seen in Figure 13. The results clearly depicted that numerically predicted results of velocity-decay plot along the axial direction matches with that of the literature.

RESULTS AND DISCUSSION

The present study numerically investigates the effect of outlet thickness and outlet angle of the bladeless fan for different aerofoil profiles namely, Eppler 169, Eppler 473, Eppler 479, S1046 and S1048. The aerofoil's outlet thickness and outlet angle have a significant impact on the bladeless fan's discharge flow ratio. The bladeless fan's performance has been optimized using a three-dimensional numerical study for various outlet angles and outlet thicknesses. The outlet thickness is varied between 0.8, 1.0, 1.3, 1.5 and 2.0 mm and slit angle is also varied between 20°, 30°, 40°, 50°, 60°, 70° and 80°. The discharge flow ratio of a bladeless fan has been recorded at a distance of 3Dh the aerofoil's hydraulic diameter (D_h) from its leading edge. The outlet volumetric flow rate has been recorded in a meridian plane where the diameter of the plane is found to be 1000 mm, and which is as shown in Figure 14. The velocity contours of S1046 with outlet thickness and outlet angle of 1 mm and 50 degree and the volumetric flow at inlet is maintained as 80 LPS revealed that flow velocity at the core region is around 4.0 m/s approximately and the fluid flow velocity measured near the slit-region is around 100 m/s. This clearly shows that high velocity jet flow near the slit area tends to decay

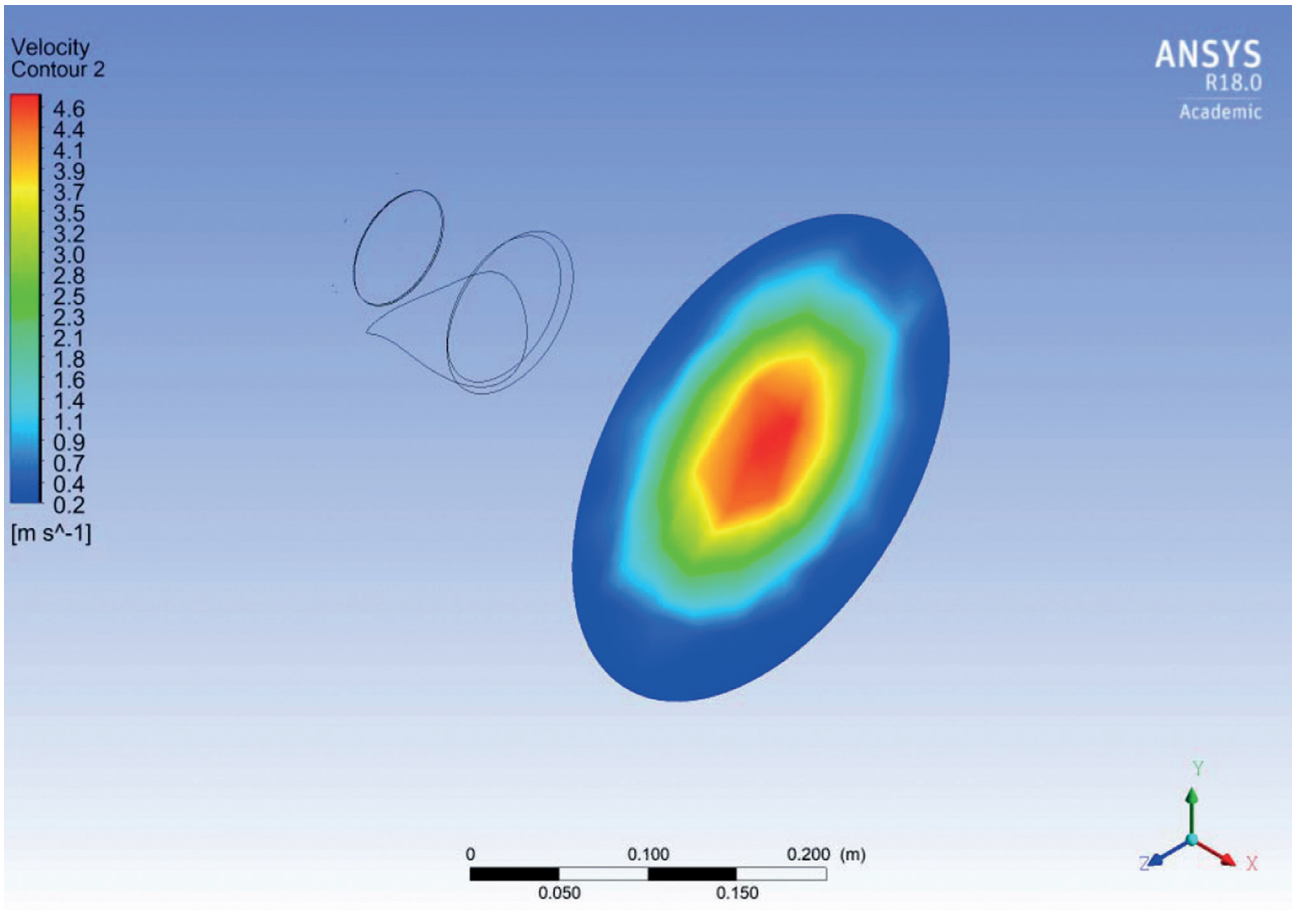

Figure 14. Velocity contour at circular plane for a S1046 profile with an outlet thickness of 1 mm.

along the air-flow direction. The flow stabilises and reaches a similarity state when the distance away from the leading-edge beyond 3.5 times the hydraulic diameter. Hence, in this present study, a meridian plane is used to measure the volumetric flow rate at a minimum distance that is 3Dh the hydraulic diameter (D_h) and the diameter of the circular plane corresponds to 1000 mm [9, 16]. It has been observed from the present study, that when the outlet thickness decreased from 2 mm to 1 mm the discharge flow ratio of bladeless fan has increased up to 32. As the thickness of the slit has been reduced from 2 mm to 1 mm, the area of the slit becomes smaller which would tremendously increase the exit air velocity and decreases the pressure through and around the aerodynamic ring region. When the thickness of the slit gradually decreases, the pressure variation between the surrounding and aerodynamic ring regions increases. This pressure gradient drives the suction air to flow along with the inlet air and thereby increases the discharge flow ratio. The maximum discharge flow ratio has been recorded from the literature so far is around 21 [10] only, whereas a discharge flow ratio of roughly 32 was achieved for the E473 aerodynamic profile with a 1 mm outlet thickness and a 70 degree outlet angle. Thus from the present study, comparing the performance of a bladeless fan with the existing literature, an improvement of more than 34.37% has been observed.

Effect of Aero Foil Profiles

In this section, the effect of various aerodynamic profiles namely, Eppler169, Eppler473, Eppler479, S1046 and S1048 have been numerically investigated. The outlet angle and outlet thickness of the bladeless fan has been fixed constant as 20 degrees and 2 mm respectively and the inlet volumetric flow rate has been adjusted from 5 LPS to 80 LPS. The discharge flow ratio for variation in inlet volumetric flow rates have been compared and presented for various aerodynamic profiles as shown in Figure 15. The results revealed that the Eppler473 aero foil showed a maximum discharge flow ratio of 22 and this corresponds to the outlet volumetric flow rate of 1770 LPS for an inlet volumetric flow rate of 80 LPS. The discharge flow ratio for the other aerodynamic profiles namely, S1048, S1046, Eppler 479

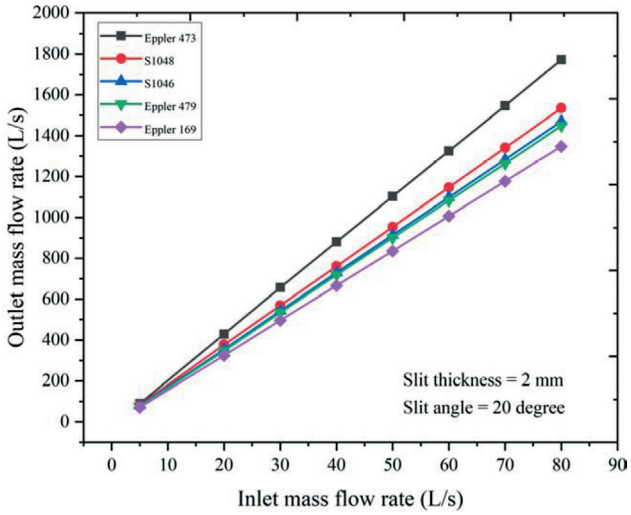

Figure 15. Discharge flow ratio of various aerodynamic profiles with an outlet thickness of 2 mm.

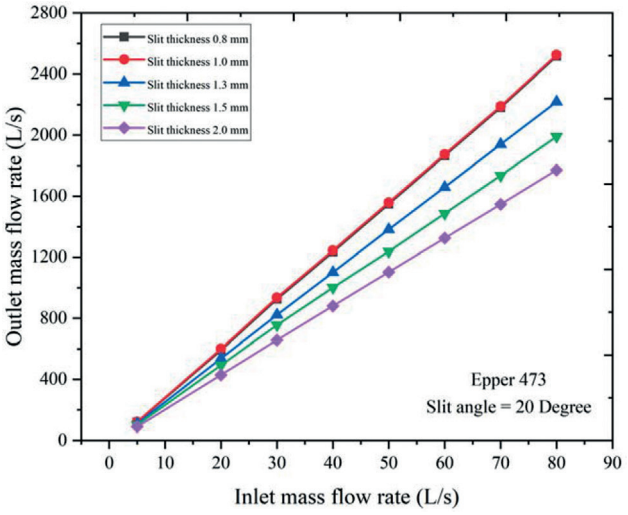

Figure 16. Eppler 473 discharge flow ratio for various outlet thicknesses with outlet angle of 20 degree.

and Eppler 169 have been recorded as 19.2, 18.4, 18.10 and 16.84 which corresponds to the outlet volumetric flow rate of 1535, 1470, 1450 and 1350 LPS respectively.

The discharge flow ratio for the Eppler 473 aerofoil has been increased by 13%, 16.4%, 17.8% and 23.5% when compared with the S1048, S1046, Eppler 479 and Eppler 169 aerofoil profiles respectively. This clearly shows that Eppler 473 aerofoil profile is the best suitable aerofoil among the other aerofoils presented in this study, when the outlet thickness and slit angle has been maintained as 2 mm and 20 degree respectively. Hence Eppler 473 aerodynamic profile has been considered for the further studies and the numerical analysis has been extended for various thicknesses varying between 0.8 mm and 2 mm.

Effect of Outlet Thickness

The first phase of the numerical analysis, which is covered in this section, examines whether the outlet thickness influences the performance of the Eppler 473 aerofoil. The thickness of the slit has been varied between 0.8 mm and 2 mm. Figure 16 illustrates the discharge flow ratio compared and presented for the Eppler 473 aero foil profile for the various thicknesses mentioned above and the outlet angle has been maintained as 20 degrees. The results revealed that reducing the thickness of slit provided a drastic improvement in the outlet volumetric flow rate. The volumetric flow rate of 1770 LPS has been recorded at outlet when the thickness of the slit maintained at 2 mm. Further, the thickness of the slit has been reduced to 1.5, 1.3, and 1 mm, the volumetric flow rate at outlet has been noted as 1990, 2220 and 2530 LPS respectively for a constant inlet volumetric flow rate of 80 LPS. When the thickness of the slit is reduced beyond 1 mm to 0.8 mm the outlet volumetric flow rate shows a negative trend, i.e. a decline in the volumetric flow rate at outlet from 2530 to 2520 LPS. The maximum discharge flow ratio is calculated for different thicknesses namely, 2, 1.5, 1.3, 1 and 0.8 mm which corresponds to 22, 24.8, 27.7, 32 and 31.5. As a result, the optimal outlet thickness of the bladeless fan has been set at 1 mm for further studies. Thus, when the thickness of the slit is reduced from 2 mm to 1 mm the maximum discharge flow ratio has been increased by 32.25% for the Eppler473 aerodynamic profile at a constant slit angle of 20 degree and the volumetric flow rate at inlet has been maintained as 80 LPS.

In the second part of this section, the numerical simulation has been carried out extensively in order to substantiate that Eppler 473 is the best suitable aerodynamic profile over the other aerodynamic profiles for all the outlet thickness values considered in the numerical investigation. Hence, the impact of outlet thickness (0.8, 1.0, 1.3, 1.5 and 2 mm) have been investigated for all the aerofoil profiles namely S1046, S1048, Eppler479, Eppler473 and Eppler169 and the results have been thoroughly discussed and presented. The maximum discharge flow ratio of Eppler169, Eppler473, Eppler479, aerodynamic profiles has been compared and presented against various outlet thicknesses as shown in Figure 17. The discharge flow ratio increases from 22 to 32 when the Eppler 473's outlet thickness is reduced from 2 mm to 1 mm. A similar trend is observed for the rest of aerodynamic profiles namely Eppler169, Eppler479, S1046 and S1048 and maximum discharge flow ratio has been increased to 16.83 to 29, 18.1 to 29, 18.37 to 28.77 and

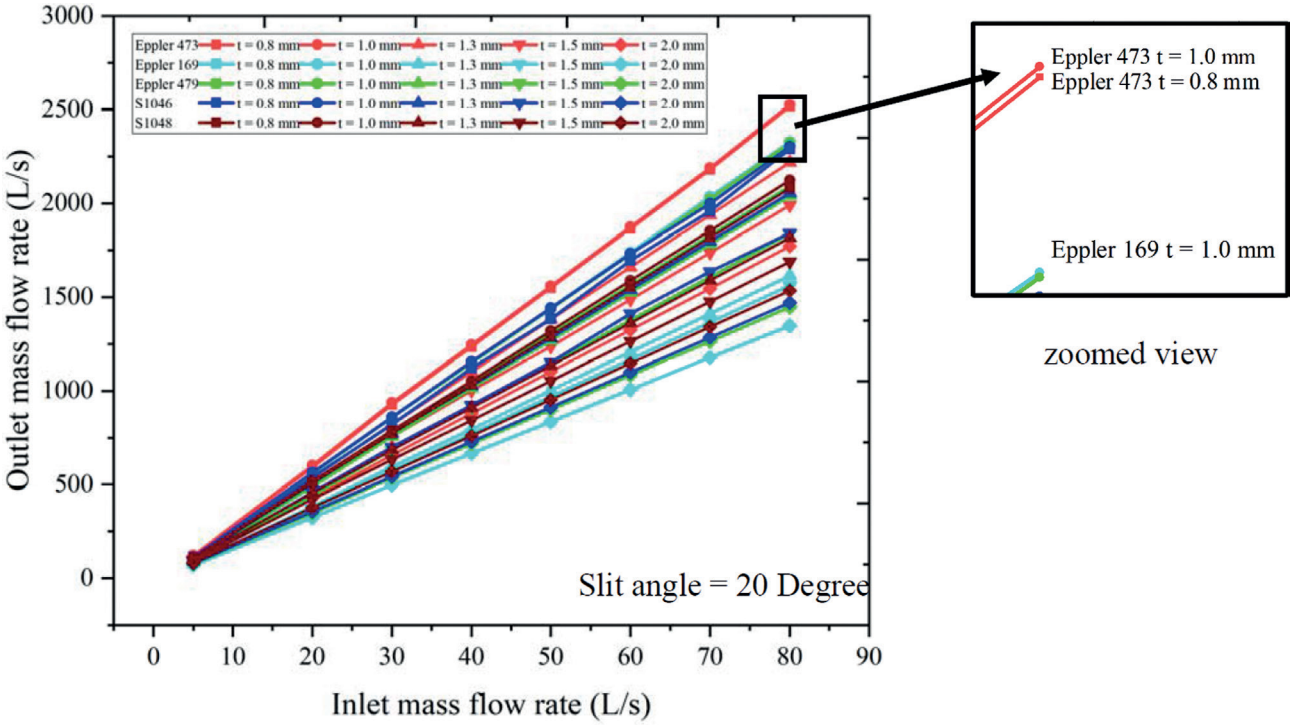

Figure 17. Discharge flow ratio of various aerodynamic profiles with varying thicknesses.

19.17 to 26.54 respectively when the thickness has been reduced from 2 mm to 1 mm. Thus it has been observed for any aerodynamic profile the discharge flow ratio is recorded when the outlet thickness is 1 mm and found to be maximum for Eppler 473 aero foil at a outlet angle of 20° as shown in zoomed view of Figure 17. The maximum discharge flow ratio of Eppler 169 is lesser by 7.9% to that of Eppler 473 profile for the same outlet thickness of 1 mm and the outlet angle is maintained as 20°. Similarly the discharge flow ratio recorded for Eppler 479, S1046 and S1048, has been reduced by 8.1%, 8.86% and 15.95% respectively to that of E473 aerodynamic profile for an outlet thickness value of 1 mm.

Effect of Outlet Angle

The first part of the numerical analysis, which is covered in this section, examines whether the outlet angle influences the performance of the Eppler473 aerodynamic profile for the optimized outlet thickness value of 1 mm. The outlet angle has been adjusted between 20 degrees and 80 degrees with an increment of 10 degree. Figure 18 represents the discharge flow ratio plot for various outlet angles of an Eppler473 aerodynamic profile with an outlet thickness of 1 mm. The volumetric flow rate measured at outlet has been recorded as 2530, 2535, 2553, 2579, 2714, 2748 and 2733 LPS for the outlet angle of 20°, 30°, 40°, 50°, 60°, 70° and

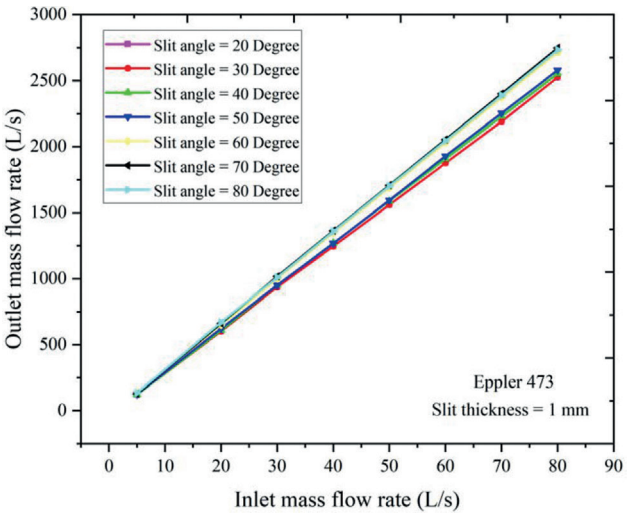

Figure 18. Eppler 473 discharge flow ratio for various outlet angles with a 1 mm outlet thickness.

80° respectively. It has been found that for the Eppler473 aerodynamic profile, the discharge flow ratio increases by 8.78% when the slit angle is raised from 20 to 70, resulting to an additional 220 LPS of exit volumetric flow rate at the

larger slit angle. Thus the results clearly predicted that when the outlets angle is increased from 20 degrees to 70 degrees, the maximum discharge flow ratio of the bladeless fan also increases from 32 to 34.35 and increasing further the outlet angle to 80 degree reduces the discharge flow ratio very marginally to 34.16 from 34.35. This decrease in discharge flow ratio from 34.35 to 34.16 may be due to the separation of airflow or detachment of air flow along the aerofoil section commonly termed as stalling phenomenon. Therefore, the optimized outlet thickness and outlet angle of the bladeless fan for Eppler 473 aerodynamic profile is found to be 1 mm and 70 degree respectively

The numerical investigation was extended in order to the study to substantiate that the Eppler 473 aerofoil with outlet angle of 70 degree and outlet thickness of 1 mm is the best configuration arrived among all the aerofoil profiles considered as the outlet angle has been maintained between 20 degree and 80 degree. The effect of outlet angle has been adjusted between 20 degrees and 80 degrees have been numerically investigated for all the aerofoil profiles considered and thickness of the slit has been maintained as 1 mm. The numerical results have been thoroughly discussed and presented. Figure 19 presents the discharge flow ratio of Eppler473 compared and presented and the same has been compared with other aerodynamic profiles of Eppler169, Eppler479, S1046, and S1048 for various slit angles. In comparison to the other aerodynamic profiles taken into consideration, the Eppler473 aerofoil provides the maximum discharge flow ratio of 2750 LPS with a outlet thickness of 1 mm and slit angle of 70 degrees. When the outlet angle has increased from 20° to 70°, the discharge flow ratio of all the aerodynamic profiles namely Eppler169, Eppler479, S1046 and S1048 has increased by 5.6%, 7.1%, 9.0%, and 9.93%, respectively.

The discharge flow ratio tends to increase from 32 to 34.37 when the Eppler 473's outlet angle has increased from 20 degrees to 70 degrees. A common pattern can be noticed for the rest of the aerodynamic profiles namely, Eppler169, Eppler479, S1046 and S1048 with maximum discharge flow ratio tending to increase from 22 to 25.98, 29 to 31.1, 28.77 to 31.37 and 26.54 to 29.17 respectively, when the outlet angle is increased to 70 degrees from 20 degrees. The maximum volumetric flow rate at outlet has been recorded for all the aerodynamic profiles namely, S1046, S1048, Eppler473, Eppler169 and Eppler479 with outlet thickness of 1 mm are 2629, 2334, 2750, 2079 and 2552 LPS respectively for outlet angles ranging from 20 degrees to 80 degrees. From the results, it has been observed that for the Eppler473 aerofoil at an outlet angle of 70°, provided the maximum outlet volumetric flow rate of 2750 LPS and maximum discharge

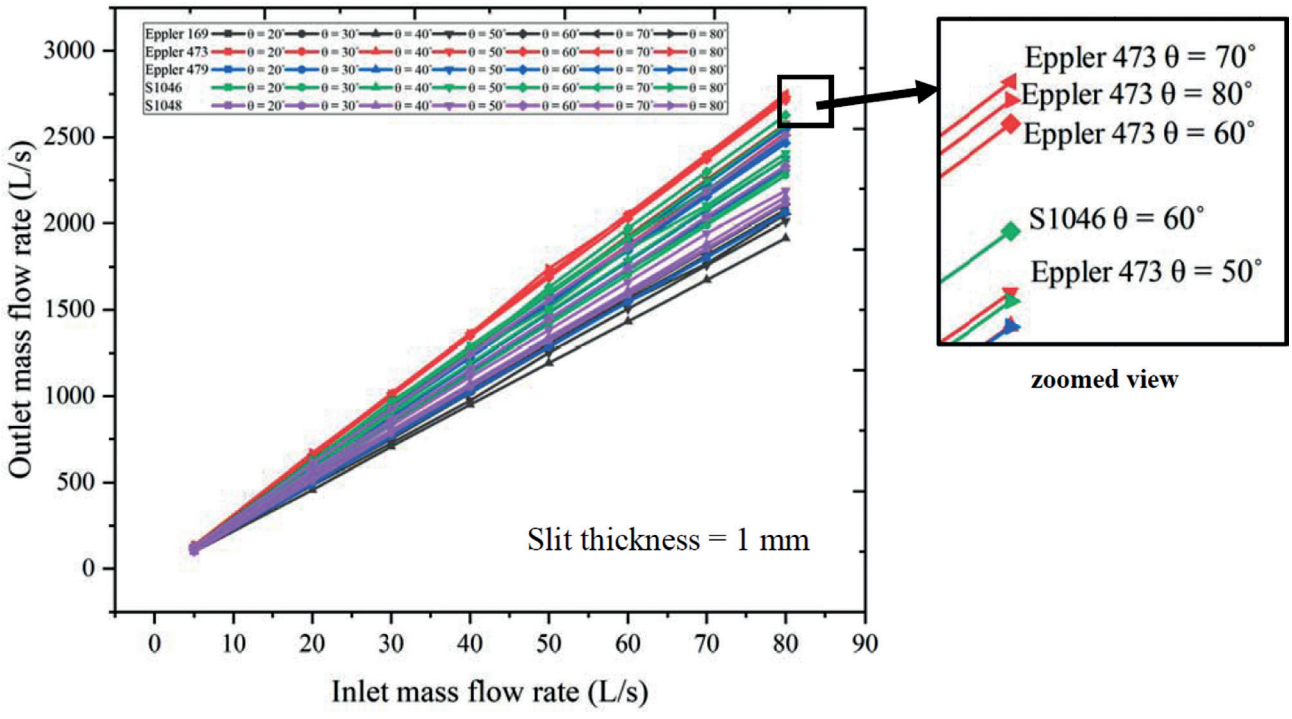

Figure 19. Discharge flow ratio for various aerodynamic profiles for slit angles with a outlet thickness of 1 mm.

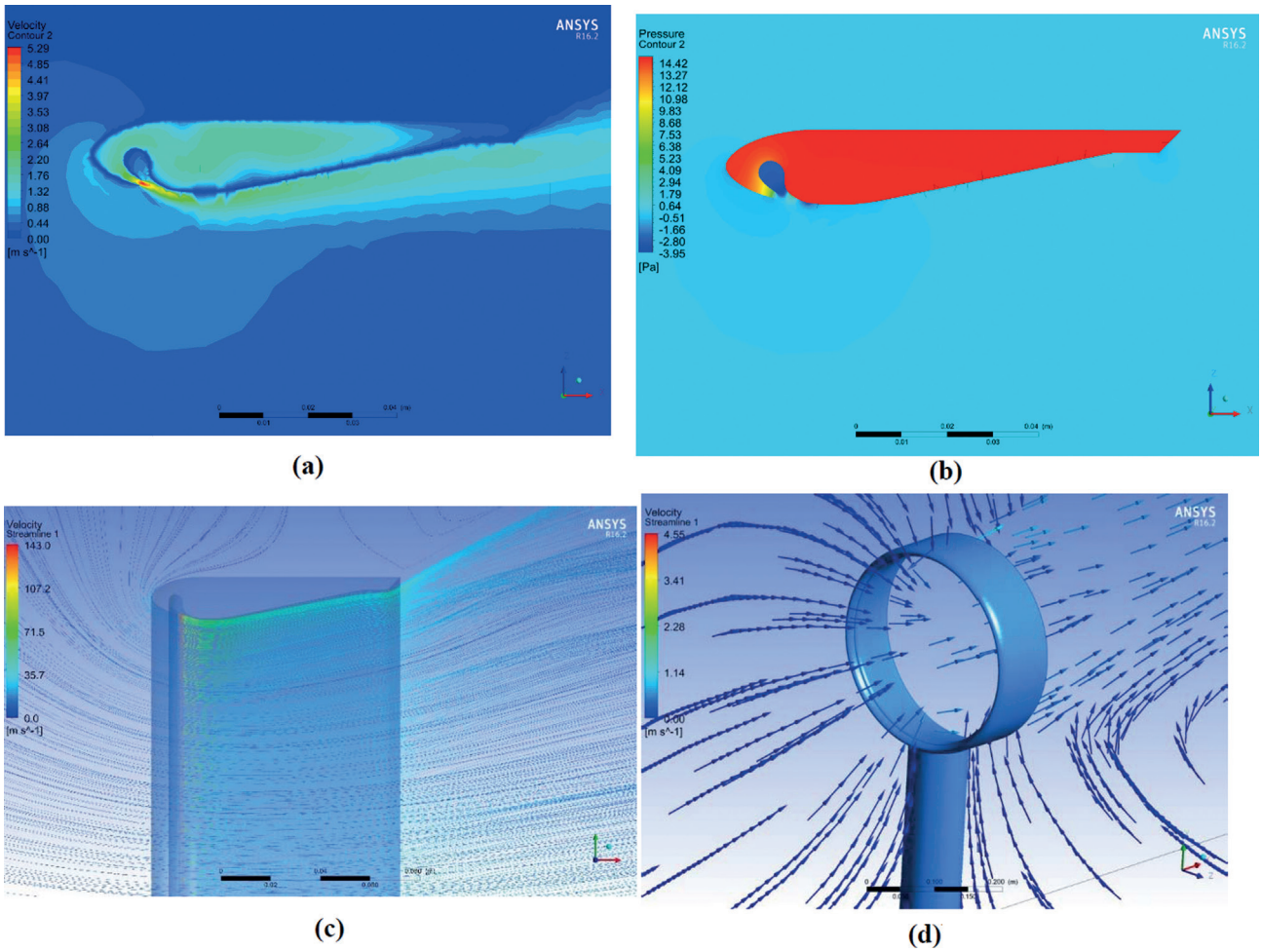

Figure 20. (a) Velocity plot of Eppler 473 (t = 1 mm) for 5 LPS, (b) Pressure plot of Eppler 473 (t = 1 mm) for 5 LPS, (c) Streamline around the bladeless fan of E473 for t = 1 mm for 80 LPS, (d) Velocity vector contour for the Eppler473 for t = 1 mm for 5 LPS.

flow ratio of 34.37 are obtained of all the configurations considered in this work. This is highlighted in the zoomed view of Figure 19.

The contours of velocity, pressure, streamline and velocity vector for an Eppler473 aerofoil with an outlet angle and outlet thickness values of 70 degrees and 1 mm respectively for an inlet volumetric flow rate of 5 LPS as seen in Figure 20 (a). The high speed fluid jet velocity of nearly 143 m/s is observed near the slit area and this tends to decrease along the flow direction as seen in Figure 20 (c) for 80 LPS. It can be seen in Figure 20 (b), the annular ring region experiences a pressure drop below atmospheric as a result of the high-speed jet flow that emerges from the slit. As depicted in Figure 20 (c), the bladeless fan's pressure fluctuations between the aerodynamic ring and the surrounding air forces the air to pass through around the aerodynamic ring region. The streamlines in Figure 20 (c) depict the forced flow that takes place within and around the annular ring region as the atmospheric air from the bladeless fan is collected and forced to flow across the aerodynamic ring. Figure 20(d) depicts the velocity-vector plot for an Eppler473 using an optimized outlet thickness of 1 mm and an optimized slit angle of 70 degrees to clearly comprehend the fluid-flow behaviour and air flow direction.

CONCLUSION

The effect of outlet thickness and outlet angle on bladeless fan performance has been carried out numerically. The aerodynamic profile, thickness of the slit and outlet angle has been investigated in detail. The thickness of slit has been maintained between 2 mm and 0.8 mm and the outlet angle has been maintained between 20 degrees to 80 degrees for all the aerodynamic profiles namely, S1046, S1048, E169, E479 and E473 have been investigated in this present work.

1. The results from the study predicted that Eppler 473 aerodynamic profile provided better performance than the other aerodynamics profiles namely S1046, S1048, E169, E479 considered.
2. The results revealed that reducing thickness of the slit from 2 mm to 1 mm offered a maximum discharge flow ratio of 32 respectively for an E473 aerodynamic profile.
3. The results revealed that increasing the outlet angle for Eppler473 aerodynamic profile from 20 degrees to 70 degrees, discharge ratio tends to increase and also it is observed that the discharge flow ratio of all aerofoil have increased with increase of outlet angle for the outlet thickness value of 1 mm.

Thus, it can be inferred from the study that the E473 aerodynamic profile with an outlet thickness of 1 mm and outlet angle of 70 offered a discharge flow ratio of 34.37 for an inlet volumetric flow rate of 80 LPS.

NOMENCLATURE

dB sound pressure level, decibel, dB
CFD Computational Fluid Dynamics
C_l lift coefficient
C_d drag coefficient
D cylinder diameter, mm
E Eppler
m mass flux kg/s
p static-pressure, Pa
p_{atm} atmosphere-pressure, Pa
t outlet thickness, mm
u x-component velocity, m/s
U_{in} Velocity at inlet, m/s
U_{cl} core velocity, m/s
V velocity, m/s
v y component velocity, m/s
w z component velocity, m/s
x distance from leading edge of an aerofoil, mm

Greek symbols:
k turbulence kinetic energy, $m^2 s^{-2}$
α angle of attack, degree
ρ density, kg m^{-3}
μ dynamic viscosity, kg m/s
ω turbulent dissipation rate, $m^2 s^{-3}$
θ outlet angle, degree
μT turbulent viscosity, $m^2 s^{-1}$

AUTHORSHIP CONTRIBUTIONS

Authors equally contributed to this work.

DATA AVAILABILITY STATEMENT

The authors confirm that the data that supports the findings of this study are available within the article. Raw data that support the finding of this study are available from the corresponding author, upon reasonable request.

CONFLICT OF INTEREST

The author declared no potential conflicts of interest with respect to the research, authorship, and/or publication of this article.

ETHICS

There are no ethical issues with the publication of this manuscript.

REFERENCES

[1] Gammack PD, Nicolas F, Simmonds KJ. United States Patent. No: US 8,308,445 B2. Nov. 13, 2012.
[2] Krömer FJ, Moreau S, Becker S. Experimental investigation of the interplay between the sound field and the flow field in skewed low-pressure axial fans. J Sound Vib 2019;442:220–236. [CrossRef]
[3] Scheit C, Karic B, Becker S. Effect of blade wrap angle on efficiency and noise of small radial fan impellers - A computational and experimental study. J Sound Vib 2012;331:996–1010. [CrossRef]
[4] Chunxi L, Ling WS, Yakui J. The performance of a centrifugal fan with enlarged impeller. Energy Convers Manag 2011;52:2902–2910. [CrossRef]
[5] Moosania M, Chao ZH, Site HU. Effect of tip geometry on the performance of low-speed axial flow fan. Int J Refrig 2022;134:16–23. [CrossRef]
[6] Guoqi L, Peifeng L, Baoling C, Yingzi J, Yongjun H, Zhe L. Numerıcal sımulatıon on flow field of bladeless fan. In: Proceedings of the ASME 2014 4th Joint US-European Fluids Engineering Division Summer Meeting. 2014. p. 1–7. [CrossRef]
[7] Li G, Hu Y, Jin Y, Setoguchi T, Kim HD. Influence of Coanda surface curvature on performance of bladeless fan. J Therm Sci 2014;23:422–431. [CrossRef]
[8] Jafari M, Afshin H, Farhanieh B, Sojoudi A. Numerical investigation of geometric parameter effects on the aerodynamic performance of a Bladeless fan. Alexandria Eng J 2016;55:223–233. [CrossRef]
[9] Jafari M, Afshin H, Farhanieh B, Bozorgasareh H. Experimental and numerical investigation of a 60cm diameter bladeless fan. J Appl Fluid Mech 2016;9:935–944. [CrossRef]
[10] Li H, Jin XH, Deng HS, Lai YB. Experimental investigation on the outlet flow field structure and the influence of Reynolds number on the outlet flow field for a bladeless fan. Appl Therm Eng 2016;100:972–978. [CrossRef]
[11] Jafari M, Afshin H, Farhanieh B, Bozorgasareh H. Numerical aerodynamic evaluation and noise

investigation of a Bladeless fan. J Appl Fluid Mech. 2015;8:133–142.

[12] Chou TM, Lin SY, Jinn HK. A numerical study of the 3-dimensional turbulent flow past a bladeless fan. Proc - 2015 3rd Int Conf Robot Vis Signal Process RVSP 2015. 2016:240–243. [CrossRef]

[13] Mehmood K, Shahzad A, Masud J, Akram F, Mumtaz MN, Shams TA. Numerical analysis of bladeless ceiling fan: an effective alternative to conventional ceiling fan. J Wind Eng Ind Aerodyn 2022;221:104905. [CrossRef]

[14] Carlini M, Mennuni A, Rotondo M, Morelli S. Numerical simulation of innovative air capture systems based on bladeless technology with Coandă effect. J Fluid Flow, Heat Mass Transf 2022;9:1–9. [CrossRef]

[15] Aslam H, Arif MZ, Ali M, Javed A. Design and CFD analysis of bladeless ceiling fan. Proc 18th Int Bhurban Conf Appl Sci Technol IBCAST 2021. 2021:782–787. [CrossRef]

[16] Ravi D, Rajagopal TKR. Numerical investigation on the effect of geometric shape and outlet angle of a bladeless fan for flow optimization using CFD techniques. Int J Thermofluids 2022;15:100174. [CrossRef]